## Title

Outcome-related metabolomic patterns from 1H/31P NMR after mild hypothermia treatments of oxygen-glucose deprivation in a neonatal brain slice model of asphyxia.



## Journal

Journal of cerebral blood flow and metabolism : official journal of the International Society of Cerebral Blood Flow and Metabolism, 31(2)

## ISSN

0271-678X

## Authors

Liu, Jia
Litt, Lawrence
Segal, Mark R
et al.

## Publication Date

2011-02-01

## DOI

10.1038/jcbfm.2010.125

Peer reviewed

JCBFM Open

Journal of Cerebral Blood Flow & Metabolism (2011) 31, 547–559

www.jcbfm.com

# Outcome-related metabolomic patterns from $^{1}H/^{31}P$ NMR after mild hypothermia treatments of oxygen–glucose deprivation in a neonatal brain slice model of asphyxia

Jia Liu[1], Lawrence Litt[1], Mark R Segal[2], Mark JS Kelly[3], Hikari AI Yoshihara[3] and Thomas L James[3]

[1]*Department of Anesthesia, University of California, San Francisco, California, USA;* [2]*Department of Epidemiology and Biostatistics, University of California, San Francisco, California, USA;* [3]*Department of Pharmaceutical Chemistry, University of California, San Francisco, California, USA*

**Human clinical trials using 72 hours of mild hypothermia (32°C–34°C) after neonatal asphyxia have found substantially improved neurologic outcomes. As temperature changes differently modulate numerous metabolite fluxes and concentrations, we hypothesized that $^{1}H/^{31}P$ nuclear magnetic resonance (NMR) spectroscopy of intracellular metabolites can distinguish different insults, treatments, and recovery stages. Three groups of superfused neonatal rat brain slices underwent 45 minutes oxygen–glucose deprivation (OGD) and then were: treated for 3 hours with mild hypothermia (32°C) that began with OGD, or similarly treated with hypothermia after a 15-minute delay, or not treated (normothermic control group, 37°C). Hypothermia was followed by 3 hours of normothermic recovery. Slices collected at different predetermined times were processed, respectively, for 14.1 Tesla NMR analysis, enzyme-linked immunosorbent assay (ELISA) cell-death quantification, and superoxide production. Forty-nine NMR-observable metabolites underwent a multivariate analysis. Separated clustering in scores plots was found for treatment and outcome groups. Final ATP (adenosine triphosphate) levels, severely decreased at normothermia, were restored equally by immediate and delayed hypothermia. Cell death was decreased by immediate hypothermia, but was equally substantially greater with normothermia and delayed hypothermia. Potentially important biomarkers in the $^{1}H$ spectra included PCr-$^{1}H$ (phosphocreatine in the $^{1}H$ spectrum), ATP-$^{1}H$ (adenosine triphosphate in the $^{1}H$ spectrum), and ADP-$^{1}H$ (adenosine diphosphate in the $^{1}H$ spectrum). The findings suggest a potential role for metabolomic monitoring during therapeutic hypothermia.**
*Journal of Cerebral Blood Flow & Metabolism* (2011) **31,** 547–559; doi:10.1038/jcbfm.2010.125; published online 18 August 2010

**Keywords:** brain slice; hypothermia; immunohistochemistry; NMR spectroscopy; neonatal ischemia; oxygen-glucose deprivation (OGD)

## Introduction

Two large randomized clinical trials recently found that after neonatal asphyxia, 72 hours of mild brain hypothermia (33°C to 34°C), begun no more than 6 hours after birth, improves long-term neurologic outcome. In the CoolCap study (Gluckman *et al*, 2005; Gunn *et al*, 1998), the scalp and underlying tissues were cooled, whereas in a larger clinical trial (Shankaran *et al*, 2005), the whole body was cooled. This together with other evidence in human newborns of improved neurologic outcomes (Compagnoni *et al*, 2002, 2008) has initiated a 'surge' in mechanism-oriented hypothermia research projects. We believe that important issues related to optimal cooling temperatures, durations, rewarming regimens, and mechanisms—and to the individualization of therapy—would be better addressed if there were a reliable way to identify and assess helpful and harmful intracellular events during the many hours of a hypothermia treatment.

We also believe that magnetic resonance spectroscopy (or nuclear magnetic resonance (NMR) spectroscopy) has enormous potential for ultimately guiding therapeutic hypothermia in humans. One of several NMR approaches involves *metabolic*

Correspondence: Dr L Litt, Department of Anesthesia 0648, University of California, 521 Parnassus Avenue, Rm C455, San Francisco, CA 94143-0648, USA.
E-mail: littl@anesthesia.ucsf.edu
This study was supported by NIH award R01 GM34767.
Received 6 April 2010; revised 2 July 2010; accepted 5 July 2010; published online 18 August 2010

*profiling*, or *NMR metabolomics* (sometimes referred to as *metabonomics*), in which ensembles of NMR metabolites, 49 in this study, are subjected to multivariate analyses. As hypothermia differently modulates the fluxes and concentrations of numerous metabolites, it is reasonable to ask whether substantial physiological changes that come from a 4°C temperature change are associated with impressive metabolic variations and changes in the characteristics of specific metabolite ensembles. Such might occur if important chemical activation energy thresholds undergo large changes in the 4°C temperature range, as suggested by the Arrhenius equation (as explained in the Appendix).

Methodological advances have already made it possible to accurately obtain *in vivo* 14.1 Tesla NMR quantifications in mice of 19 $^{1}$H metabolites (Lei *et al*, 2010; Mlynarik *et al*, 2008) and also to use such methods to perform ischemia studies (Berthet *et al*, 2009). Although safety and other issues augment the challenges of doing high field, *in vivo* NMR studies of neonates and infants (De Vita *et al*, 2006; Dagia and Ditchfield, 2008), one can still have the hope that such will ultimately be available for individualizing treatments with therapeutic hypothermia.

As an early step toward *in vivo* goals, we have performed *ex vivo* experiments using a neonatal (P7) rodent brain slice model, where insults, treatments, and outcomes can be clearly defined and regulated. Asphyxia was modeled by oxygen–glucose deprivation (OGD), and two hypothermia protocols were studied, along with a normothermia control. Tissues were removed during and after hypothermia, and high-resolution 14.1 Tesla $^{1}$H/$^{31}$P NMR spectroscopy was used to determine changes in perchloric acid extracted metabolite concentrations. We asked whether NMR metabolic profiles of metabolite ensembles could accurately differentiate treatments, and good from bad outcomes, these being defined via quantifications of cell death and ATP preservation, with superoxide production helping to provide assessments of OGD insults.

## Materials and methods

### Cerebrocortical Slice Acquisition and Superfusion

All animal experiments were approved by UCSF's Institutional Animal Care and Use Committee. Slice preparation protocols were as described previously (Espanol *et al*, 1992; Zeng *et al*, 2007; Liu *et al*, 2008, 2009), with 20 350-$\mu$m cerebrocortical slices coming from 10 anesthetized 7-day-old Sprague-Dawley rat littermates of either sex. Excised slices were placed immediately in a superfusion chamber containing fresh, oxygenated artificial cerebrospinal fluid (oxy-ACSF) that consisted of a modified Krebs balanced salt solution: 124 mmol/L NaCl, 5 mmol/L KCl, 1.2 mmol/L $KH_2PO_4$, 1.2 mmol/L $MgSO_4$, 1.2 mmol/L $CaCl_2$, 26 mmol/L $NaHCO_3$, and 10 mmol/L glucose. Continuous bubbling of oxy-ACSF with carbogen (95% $O_2$, 5% $CO_2$) maintained constant values of $PO_2$ (more than $\approx$600 mm Hg), $PCO_2$ (40 mm Hg), and pH (7.4). The oxy-ACSF flow rate was 3 mL/min. The chamber was partially submerged in a water bath having a combined circulator-temperature controller (PolyScience Standard Immersion Circulator EW-12101-84, Cole-Parmer Instruments Inc., Vernon Hills, IL, USA; http://www.cole-parmer.com) that maintained temperatures at either 37°C (normothermic) or 32°C (hypothermic).

### Oxygen–Glucose Deprivation

Oxygen–glucose deprivation was initiated by replacing the post-decapitation oxy-ACSF with glucose-free ACSF that had been deoxygenated by equilibration with an anaerobic gas mixture (95% $N_2$, 5% $CO_2$) at the required temperature. During OGD, the oxygen content of the superfusate was always $<$2 mm Hg, as determined by a fiber-optic system (FOXY-R probe and SF2000 Spectrofluorometer, Ocean Optics Inc., Dunedin, FL, USA; http://www.oceanoptics.com). The OGD period of 45 minutes was followed by 6 hours of superfusion with oxy-ACSF containing 4 mmol/L glucose.

### Experimental Design

Four experiments with 45-minute OGD periods were performed for each of the three groups: (1) Normothermia (Group N), in which 37°C was maintained during OGD and a subsequent 6-hour recovery period. (2) Hypothermia (Group H), in which slices underwent a rapid temperature change from 37°C to 32°C (hypothermia) simultaneously with the onset of OGD. Hypothermia continued throughout OGD (45 minutes) and afterwards throughout 3 hours of recovery with oxy-ACSF. Following hypothermia was 1 hour of slow rewarming to 37°C, achieved by

**Abbreviations**

ADP, adenosine diphosphate
ATP, adenosine triphosphate
Ala, alanine
Asp, aspartate
Arg, arginine
Cr, creatine
GABA, 4-aminobutyrate
Leu, leucine
NAA, *N*-acetyl-aspartate
NAG, *N*-acetyl-glutamate
PCr, phosphocreatine
Phe, phenylalanine
$NADP^+$/NADPH, nicotinamide adenine dinucleotide phosphate
The, threonine
Val, valine
The addition of "-$^{1}$H" to a metabolite abbreviation denotes the quantification of that metabolite in proton spectra, rather than in phosphorous spectra.

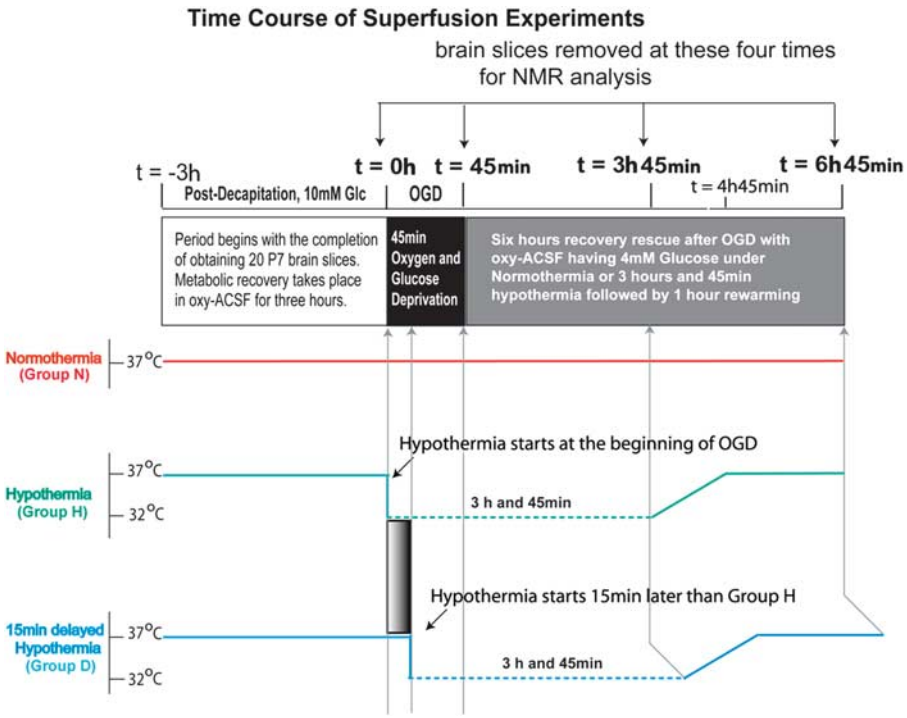


**Figure 1** Schematic diagram showing experiment time courses for each treatment group. Slice superfusion starts from the left ($t = -3$ hours). After 3 hours of metabolic recovery is completed ($t = 0$), a 45-minute oxygen–glucose deprivation (OGD) period starts, and is then followed by 6 hours of reoxygenation, with hypothermia ending at $t = 3.75$ hours. Six predetermined times are indicated above the rectangle. Brain slices were removed at the four times marked by vertical black arrows. Below the rectangle are timelines for the three experimental groups: normothermia (red), hypothermia (green), and delayed hypothermia (blue). Hypothermia and OGD began simultaneously for the middle group. The gray gradient bar between the bottom two timelines highlights the 15-minute delay that occurred before switching from a normothermic OGD superfusate to one at 32°C. Both hypothermic groups underwent the 32°C treatment for 3 hours and 45 minutes.

increasing the bath temperature 0.1°C per 1 to 1.5 minutes. Superfusion with oxy-ACSF continued at 37°C for the last 2 hours of the experiment. (3) Delayed hypothermia (Group D), where the group underwent the same cooling duration and hypothermic treatment as Group H, except for having the onset of hypothermia begin 15 minutes after the start of OGD. For all groups, five or six slices were removed from the superfusion chamber for NMR or histologic analysis at each of the four time points: before the onset of OGD ($T_0$), at the end of OGD ($T_1$), at the end of hypothermia ($T_2$), and at the end of the experiment ($T_3$). Figure 1 shows a schematic diagram of the protocol.

## Perchloric Acid Metabolite Extraction

Perchloric acid extraction and NMR tube loading were performed as described in earlier studies (Espanol *et al*, 1992; Liu *et al*, 2008, 2009). In brief, frozen slices from each time point were ground under liquid nitrogen in a precooled mortar and then extracted using 30 mL/g (dry mass) of ice-cold 12% perchloric acid. The extracts were neutralized to pH 7.0 with KOH and lyophilized for 24 hours (BenchTop 2K lyophilizer, Virtis, Gardiner, NY, USA). Before NMR analysis, lyophilized dry extracts were weighted and stored at −80°C and prepared for $^1$H spectroscopy by resuspension in 430 $\mu$L of $D_2O$ containing 0.02% 4,4-dimethyl-4-silapentane-1-sulfonic acid, a reference compound for NMR determinations of chemical shifts and signal intensities. Samples were neutralized to pD 7.0 to 7.4, with DCl before being loading into 5 mm NMR tubes (Advanced Microtube CMS-005TB matched to $D_2O$, Shigemi, Inc., Allison Park, PA, USA). After completing $^1$H NMR spectroscopy, NMR tube contents underwent the addition of EDTA and methylene diphosphonate (0.4 mmol/L). The former chelates cations that cause NMR line broadening, whereas the latter served as a $^{31}$P NMR reference. The pD was readjusted to 7.0 to 7.4 with NaOD before acquiring proton-decoupled $^{31}$P NMR spectra.

## Nuclear Magnetic Resonance Data Acquisition and Analysis

One-dimensional NMR studies of extracts were performed in the UCSF Magnetic Resonance Laboratory using a 14.1-Tesla (600 MHz) Varian UNITY spectrometer, with an INOVA console and a customized, multinuclear Z-SPECT radiofrequency probe that was optimized for this project (3NG600-8, Nalorac Division of Varian, Martinez, CA, USA). Basic one-pulse RF sequences, as described previously (Liu *et al*, 2009), were used for obtaining $^1$H spectra at 599.92 MHz and $^{31}$P spectra at 242.86 MHz. The extra homogeneity provided by 5 mm Shigemi NMR tubes

and the Varian INOVA shimming software typically resulted in spectral linewidths $<0.0025$ p.p.m. full width at half maximum (1.5 Hz full width at half maximum) for $^{1}$H water protons and 0.01 p.p.m. full width at half maximum for $^{31}$P in phosphocreatine. Proton spectra were composed from 64 transients, with a 4-second acquisition time and a 1-second interpulse delay. A selective saturation pulse was used to suppress the water peak. Metabolites corresponding to different chemical shifts were identified and quantified with Chenomx NMR Suite Software (version 6.0, Chenomx Inc., Edmonton, AB, Canada) using targeted profiling (Weljie *et al*, 2006) and their spectral library for 600 MHz, whose pulsing parameters were used when acquiring our spectra. For each metabolite, the targeted profiling approach involves manual simultaneous adjustment of all resonance peak clusters for that metabolite. For example, quantification of the $^{1}$H doublet resonance peak at 1.33 p.p.m. (often referred to simply as 'lactate') required manipulation of clusters for both lactate and threonine, as the latter overlaps with lactate at that chemical shift. This involved manually fitting portions of the observed spectrum by coordinating simultaneous adjustments of both lactate peaks (the doublet at 1.33 p.p.m. and the quartet at 4.12 p.p.m., with simultaneous adjustments of all three threonine peaks (the doublet at 1.33 p.p.m., the doublet at 3.58 p.p.m., and the multiplet at 4.26 p.p.m.). All chemical shift assignments for peaks and clusters were then checked against chemical shift assignments published in careful studies (Govindaraju *et al*, 2000; Willker *et al*, 1996), and also listed in computer databases at the University of Wisconsin's Biological Magnetic Resonance Data Bank (Standard Compounds; http://www.bmrb.wisc.edu/metabolomics), and at the National Institute of Advanced Industrial Science and Technology (http://www.aist.go.jp/RIODB/SDBS) in Japan. $^{31}$P and $^{1}$H relaxation time corrections were not introduced, as the same NMR pulse sequence was used for all runs of the same nucleus, and the goal of the analysis was primarily to detect large differences in each metabolite from its control value.

Metabolite signal intensities were computed relative to methylene diphosphonate or 4,4-dimethyl-4-silapentane-1-sulfonic acid, and then normalized to the weight of the dry powder that was mixed with $D_2O$ before NMR

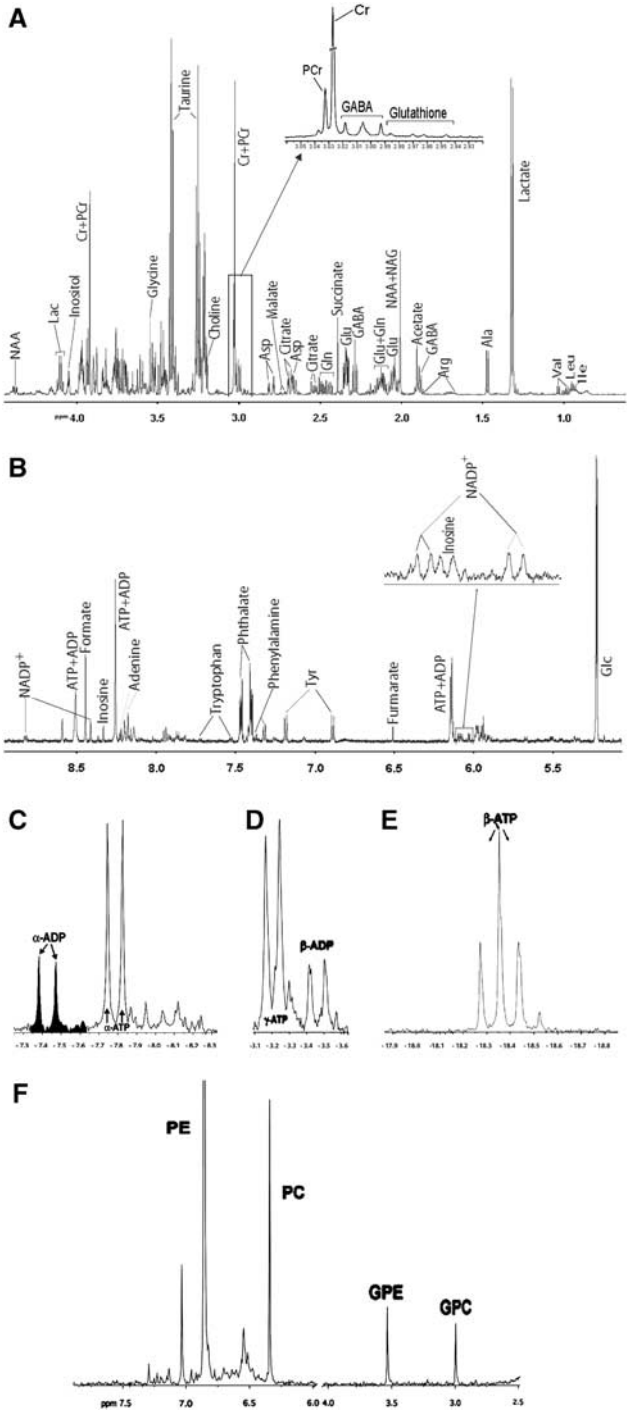


**Figure 2** (**A**, **B**) Sections of one high-resolution 600 MHz $^{1}$H nuclear magnetic resonance (NMR) spectrum of a perchloric acid extract from rat brain slices taken at $T_0$, which is just before the oxygen–glucose deprivation (OGD) insult. A 0.1-Hz line broadening was applied. Each labeled resonance peak was manually identified with Chenomx NMR Suite Software, carefully checked against online databases, and then fit, with all resonance clusters from a particular metabolite being adjusted simultaneously, as described in the text. (**A**) 0.5 to 4.5 p.p.m.: resonance peaks upfield (right side) of the water peak at 4.67 p.p.m. An enlarged insert view shows that PCr and Cr are resolvable in the $^{1}$H spectrum. Metabolite assignments are shown; (**B**) 5.0 to 9.0 p.p.m.: resonances downfield (to the left) of the water peak. Some high-energy metabolites, ATP, ADP, and NADP, can be clearly identified and quantified in this region. (**C**–**F**) Sections of a representative $^{31}$P spectrum: (**C**) The $\alpha$ADP resonance is clearly separated from the $\alpha$ATP resonance. The separated $\alpha$ADP doublet can be seen to have overlapping contributions from $\alpha$GDP, $\alpha$CDP, and $\alpha$UDP. These regions are to the right of $\alpha$ADP and their contributions are small. (**D**) The large doublet cluster is $\gamma$ATP, clearly separated from the doublet $\beta$ADP peak to its right. (**E**) A typical $\beta$ATP resonance peak is shown as a large triplet cluster at approximately $-18.4$ p.p.m. in this spectrum. The chemical shift of the sharp phosphocreatine (PCr) peak was always set at 0 p.p.m. (**F**) Four membrane-related metabolites are marked: phosphoethanolamine (PE), phosphocholine (PC), glycerol 3-phosphoethanolamine (GPE), and glycerol 3-phosphocholine (GPC).

measurements. $^{1}$H NMR spectral analysis provided quantifications of 39 metabolites: 4-aminobutyrate, ADP-1H, ATP-1H, acetate, adenine, alanine, arginine, aspartate, choline, citrate, creatine, phosphocreatine, formate, fumarate, glucose, glutamate, glutamine, glutathione, glycine, inosine, isoleucine, lactate, leucine, malate, *N*-acetylaspartate, *N*-acetylglutamate, $NADP^+$, NADPH, phosphocholine, phosphoethanolamine, phenylalanine, phthalate, succinate, taurine, threonine, tryptophan, tyrosine, valine, and myo-inositol. Figures 2A and 2B show a typical $^{1}$H NMR spectrum for extracts obtained from slices taken at $T_o$ (just before starting OGD). The insert with spectral expansion illustrates the system's outstanding $^{1}$H NMR spectral resolution by showing that the methyl protons in creatine are resolved from the methyl protons in phosphocreatine. $^{31}$P NMR spectra that were analyzed similarly, using published chemical shifts (Pettegrew *et al*, 1993), provided additional metabolite measures: ATP, ADP, phosphocreatine, phosphoethanolamine, glycerophosphoethanolamine, phosphorylcholine, and glycerophosphocholine. Overlapping $^{31}$P resonances were quantified by deconvolution with *iNMR*™ software (Mestrelab Research, Santiago de Compostela, Spain, www.inmr.net.). Figures 2C–2F display typical $^{31}$P NMR spectral peaks, also from slices taken at $T_o$.

### *In Situ* Detection of Superoxide Production

Hydroethidine (HEt; D1168, Invitrogen, Carlsbad, CA, USA) is freely permeable to living cells and selectively oxidized by the superoxide anion to red fluorescing ethidium (Et). The protocol followed the methods published in an earlier study (Liu *et al*, 2008). In brief, a parallel superfusion channel with an independent ACSF reservoir containing 5 $\mu$mol/L HEt was established for this procedure. The channel was identical to that for the original superfusion chamber, except for there being HEt in the superfusate. Thirty minutes before selected time points during perfusion of experiments, three slices were transferred from the original superfusion chamber into the parallel chamber for superfusion with ACSF containing HEt. After 30 minutes of incubation, slices were removed and fixed overnight in freshly prepared 4% formaldehyde at 4°C. On the following day, the slices were dehydrated in 30% sucrose, and then washed twice in PBS and immediately embedded in O.C.T. (Sakura Finetek Optimum Cutting Temperature compound, OpticsPlanet Inc., Northbrook, IL, USA), and cut into 10-$\mu$m-thick sections on a cryostat (Leica, CM1900, Solms, Germany). Mounting medium containing 1.5 $\mu$g/mL 4′,6′-diamidino-2-phenylindole (H1200; Vector Laboratories, Burlingame, CA, USA) was applied onto sections to counterstain cell nuclei. Superoxide anion production was assessed in a Leica SP2 Laser scanning confocal microscope at UCSF Diabetes Center's Facility for Microscopy and Cellular Imaging, with excitation wavelengths being 510 to 550 nm and emission wavelengths $>580$ nm for Et fluorescence. There was no wavelength overlap for the imaging of 4′,6′-diamidino-2-phenylindole, whose excitation and emission wavelengths are, respectively, 350 and 470 nm when bound to DNA. Quantifications of Et-positive cells were performed at five random regions between the pial layer and the injury layer of brain slices. These regions were photographed under a $\times 63$ oil immersion objective, and cell counts included neurons and glia, these not being histologically distinguishable. Counts of Et-positive cells are given as percentages of total cells counted.

### Terminal Deoxynucleotidyl Transferase-Mediated 2'-Deoxyuridine 5'-Triphosphate-Biotin Nick End Labeling Staining and Enzyme-Linked Immunosorbent Assay DNA Fragmentation Assay

Evidence for apoptosis in slices taken at different time points was examined both with fluorescence microscopy of *in situ* terminal deoxynucleotidyl transferase-mediated uridine 5′-triphosphate-biotin nick end labeling (TUNEL) staining and with quantification using a sensitive, commercial, enzyme-linked immunosorbent assay (ELISA) (Cell Death Detection ELISA$^{PLUS}$, Roche Applied Science, Indianapolis, IN, USA).

For TUNEL staining, sections were first permeabilized in 0.1% Triton X-100 (Sigma Chemical Co, St Louis, MO, USA) in PBS for 8 minutes. The TUNEL reaction mixture was obtained by adding terminal deoxynucleotidyl transferase to the nucleotide mixture according to the instructions in the manufacturer's manual (Roche Diagnostics, Mannheim, Germany). Each section was then incubated with 50 µL TUNEL reaction mixture in a humidified, dark chamber at 37°C for 60 minutes. After rinsing with PBS, sections were counterstained with 0.5 mg/mL propidium iodide to highlight nuclei. The fluorescein wavelength for excitation was 488 nm, with emissions being detected above 515 nm. Propidium iodide excitation was at wavelengths $<535$ nm, with emission being detected at $\sim 615$ nm.

The ELISA assay, which was performed according to the manufacturer's instructions, detects apoptotic but not necrotic cell death (Leist *et al*, 1998) via antibody identification of histone-associated DNA fragments. A quantitative sandwich enzyme immunoassay is performed using mouse monoclonal antibodies directed against DNA and histones. Nucleosomes, which package DNA within chromosomes, are composed of large numbers of linked histones, the proteins onto which DNA is wrapped. During apoptosis, endonuclease cleavage of double-stranded DNA occurs at the most accessible locations, the internucleosomal linker regions, thereby generating mono- and oligonucleosomes having DNA with multiples of 180 basepairs. (As the DNA within nucleosomes is tightly complexed to the histones, it is protected from cleavage during apoptosis.) The quantification by this assay is thus analogous to the quantification of 'ladder patterns' via DNA electrophoresis.

Briefly, the manufacturer's protocol involved the following: one snap-frozen cerebrocortical slice was homogenized in lysis buffer, incubated for 30 minutes, and then centrifuged. The supernatant, which contained apoptotic-related DNA fragments released from the cytoplasm, was transferred into the well of a streptavidin-coated microplate for 2 hours of incubation at room temperature. Within the well, an anti-histone antibody and an anti-DNA antibody were used to form and immobilize antibody–

nucleosome complexes. After washing and adding peroxidase substrate in the well, the anti-nucleosome complexes were quantified in a spectrophotometer with absorbance at 405 nm. To account for variations of slice size and cell numbers, spectrophotometer quantifications for each slice were normalized to the total protein concentration in that cell's lysate. The assay was performed three times for each particular time point, using three different slices, for all time points ($T_0$, $T_1$, $T_2$, and $T_3$) of each treated group.

### Statistical and Metabolomic Analyses

The NMR metabolite quantifications for all particular time points for all experimental groups underwent within-group and between-group statistical analysis. Different multivariate approaches were used, as further explained below, including: Fisher's protective least squares difference test for multiple comparisons, principal component analyses (PCA), projection to least squares discriminant analyses (PLS-DA), and the L1-penalized regression algorithm (Efron *et al*, 2004; Tibshirani, 1996).

For each time point, pairwise comparison testing for differences in individual metabolites and cell-death quantifications was performed between treatment groups. Metabolites for the last three time points were normalized to initial values, these being taken as the control in each experiment. Thus, there were nine tests for each metabolite, and also for cell-death quantifications: N (normothermia) versus D (delayed hypothermia), N versus H (hypothermia), and H versus D, that is, three comparisons for each of the times $T_1$, $T_2$, and $T_3$.

SIMCA P + v.11 software (Umetrics, Inc., San Jose, CA, USA) was used for determining PCA and PLS-DA computations. Briefly, as described in Umetrics publications (Eriksson *et al*, 2006), the SIMCA P + approach begins by mathematically creating an *N*-dimensional space, where *N* is the number of independent variables in the metabolite ensembles being compared. For comparisons of each time point's ensemble of $^{1}$H NMR metabolites, *N* is 39. When NMR data for a single time point also includes metabolites determined in $^{31}$P spectra, *N* becomes 49. Thus, each set of 39 or 49 numbers for a particular slice-removal time is represented by a single point in a 39- or 49-dimensional space. In the PCA, all metabolite data undergoes centering and unit variance scaling, after which the plane is found whose two orthogonal axes have maximum cluster separations when data points are projected onto it. Two-dimensional *scores plots* are used to display the clusters in planes where the *x* and *y* axes are principal components. In the PLS-DA, an algorithm sharpens the PCA clusters and their separations by creating a new Y variable for each data class (Eriksson *et al*, 2006). The scores plots in the PCA and PLS-DA analyses have corresponding *loadings plots* that identify metabolites that contributed most to the separations that appear in the scores plot. In the scores plot, each spectral data set is plotted as a point, which in turn defines a vector from the origin. Each such vector, however, is the vector sum of 39 or 49 smaller vectors defined by the metabolites. Projections onto the plane of the principal axes of those smaller metabolite vectors produces the *loadings plot* or *weight plot*. Although any data collection can be put through a PLS-DA analysis, the usual use in this type of study is to focus data sets that best compare outcomes. Thus, we will focus on the PLS-DA analysis for one data set, that for metabolites at the last time point (end of the experiment), with each metabolite value expressed as its ratio to the starting value (after normalization of each slice ensemble to its dry weight).

After Umetrics software processing, NMR-detected metabolites were analyzed independently with L1-penalized regression (Goeman, 2010; Tibshirani, 1996), a multivariate algorithm in which one identifies *a priori* one or more 'outcome' measures, and then, in a regression analysis, minimizes L1, the sum of absolute values of the residuals. All data for all time points are used, with identification of metabolite subsets that have the strongest influence on the 'outcome' variable(s). This was performed twice, first with there being only one outcome variable, $\beta$ATP, and then again with the only outcome variable chosen to be the cell-death measure quantified by the ELISA analysis. When taking $\beta$ATP as the outcome variable, the analysis did not include $^{31}$P-based metabolites. The motivation for using an L1 penalty (minimizing absolute deviations) in estimating regression coefficients is, in biostatistics terminology, that this specification simultaneously imparts a *shrinkage* (of the size of the set of final variables) that results both in improved predictive performance, and in a covariate selection that has improved interpretability.

The geometric underpinnings for this algorithm's behavior are detailed in Tibshirani (1996), who terms the procedure *LASSO*: Least Absolute Shrinkage and Selection Operator. However, the original LASSO algorithm can breakdown when the number of covariates (metabolites) exceeds the number of samples, as here. In such settings, the recently devised, and highly efficient, LARS (Least Angle Regression) algorithm (Efron *et al*, 2004) can be applied. Indeed, the inherent instabilities associated with small sample sizes and relatively many predictors, often correlated—as in our data sets—accentuates the importance of such shrinkage and selection. In a LARS analysis the tradeoff between model fit, which for continuous outcomes such as $\beta$ATP or the ELISA quantifications is measured via residual variance, and model complexity, arising here from the number of selected metabolites, is governed by a tuning parameter that weights the contribution of the L1 penalty. Determination of the value of the tuning parameter makes recourse to cross-validation (Hastie *et al*, 2010). Briefly, the tuning parameter value that achieves optimal fit is selected from evaluations over unseen data furnished by the cross-validation data partitioning approach. The choice of the tuning parameter determines which and how many metabolites to retained.

## Results

### High-Energy Phosphate Outcomes from $^{31}$P Nuclear Magnetic Resonance Spectra

The vertical bar plot in Figure 3A displays ATP, ADP, and PCr values for slices taken at the three experi-

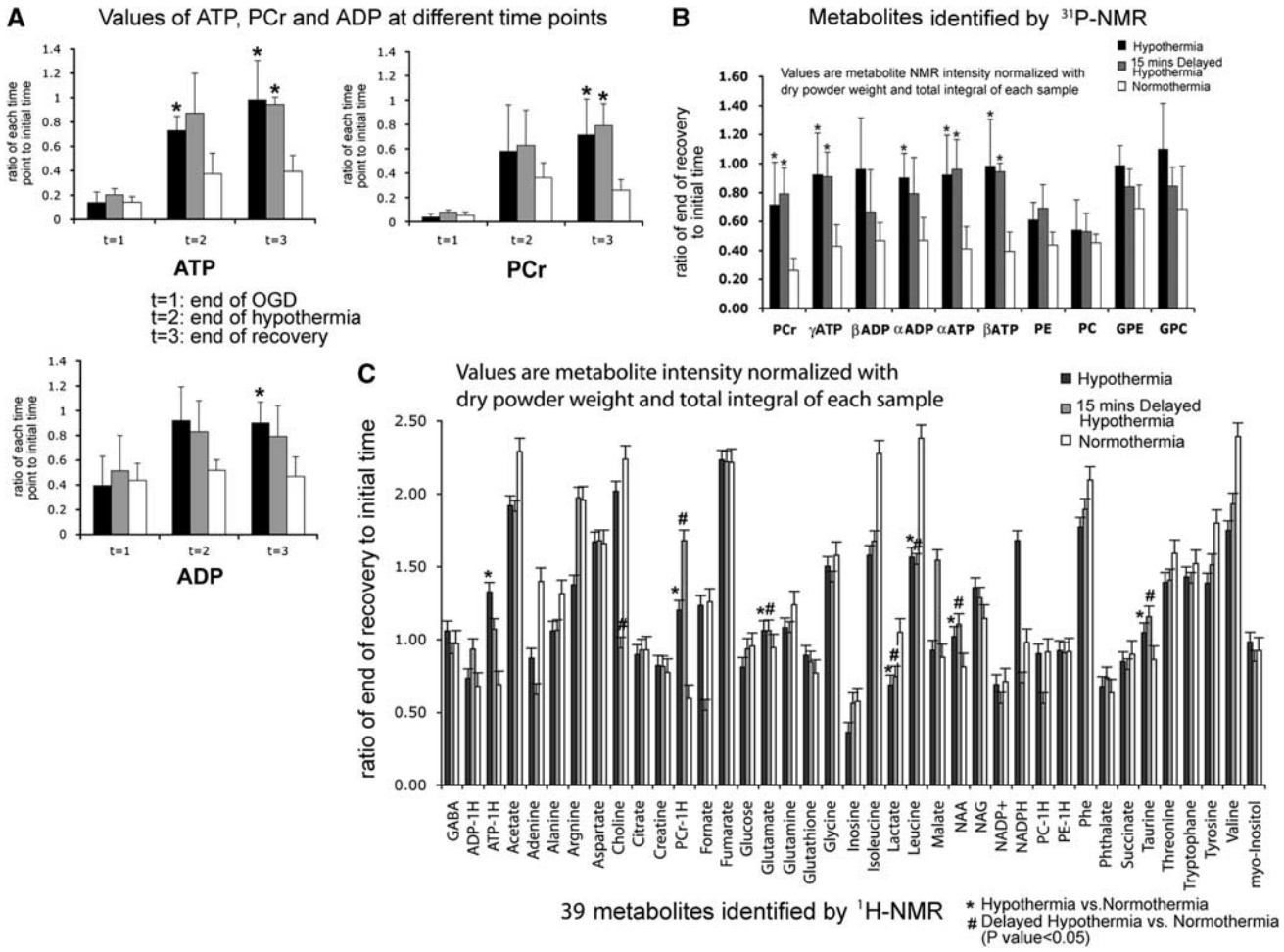


**Figure 3** $^{31}$P and $^{1}$H nuclear magnetic resonance (NMR) changes relative to control for three treated groups. See the text for computational details. (**A**) ATP, PCr, and ADP quantifications relative to control for three sampling times ($T_1$, $T_2$, and $T_3$). (**B**) Normalized final to initial ratios for the 10 $^{31}$P metabolites that were quantified. Asterisks denote statistically significant differences ($^*P < 0.05$). Data are plotted as mean ± s.d. ($n = 4$). (**C**) Normalized final to initial ratios for the 39 $^{1}$H metabolites that were quantified. Values are shown as mean ± s.e. ($n = 4$). Statistical analysis for these plots included an analysis of variance to rule out the null hypotheses, followed by the Fisher's protected least significant difference *post hoc* test.

mental time points (end of OGD, end of hypothermia, and end of experiment) measured relative to initial, pre-insult values (first time point). It shows that at the end of OGD, the time of maximal metabolic stress, ATP, ADP, and PCr decreased, respectively, to ~15%, 40%, and 5% of control. Figure 3B shows that at the end of the recovery period, that is, at the conclusion of the experiment, some 6 hours after ending OGD, values of ATP, ADP, and PCr were significantly lower in the normothermia group than in the hypothermia and delayed hypothermia groups, each of which exhibited recovery to control levels. As well, Figure 3B shows that levels of membrane phospholipids PE, GPE, PC, and GPC had similar behavior. However, it should be appreciated that when metabolite values decrease by 40%, as was the case for the final ATP for the normothermia group, NMR spectroscopy cannot distinguish between a uniform 40% loss among all cells, and the situation where 40% of the cells lost all ATP while 60% lost none.

### Metabolite Changes from $^{1}$H Nuclear Magnetic Resonance Spectra

Similar vertical bar plots for $^{1}$H metabolites, shown only for the end of the recovery period, are displayed in Figure 3C for 39 metabolites. As in the $^{31}$P NMR analysis, the level of ATP and PCr decreased substantially in the normothermia group. In addition, compared with their values in the normothermia group, NAA, glutamate, and taurine increased significantly in both the hypothermia and delayed hypothermia groups. Metabolites that were suppressed in hypothermia and delayed hypothermia groups included acetate, adenine, alanine, choline, isoleucine, lactate, leucine, tyrosine, and valine

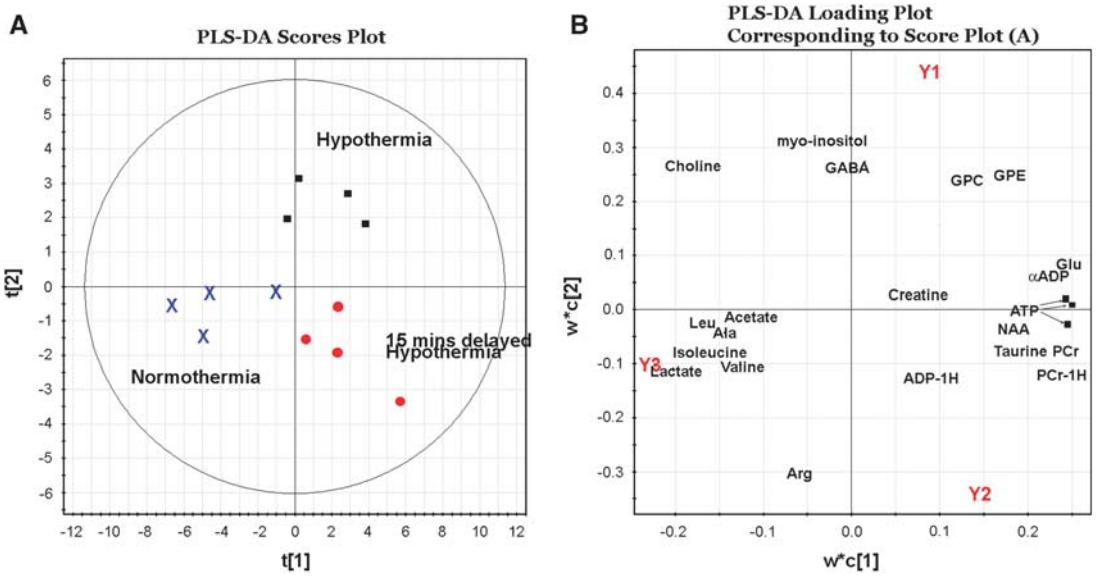


**Figure 4** (**A**) The scores plot and (**B**) the loading plot as described in the text for the final to initial metabolite ratios. (**A**) Blue X's correspond to normothermia, black squares correspond to hypothermia, and red circles correspond to delayed hypothermia. (**B**) Red letters show positions for the new Y variables defined in the SIMCA P + analysis.

(inosine and arginine decreased only in the hypothermia group).

### Metabolomic Analyses I: Projection to Least Squares Discriminant Analyses Scores and Loading Plots

Figure 4A shows the PLS-DA *scores plot* (Eriksson *et al*, 2006) produced for the final time point by the SIMCA P+ multivariate analysis, which mapped each NMR spectrum or data set into a single point in a multidimensional space, and then looked for planes where the points formed distinct clusters. The data set that resulted in Figure 4A consisted of the ratio of final to initial NMR intensities for each metabolite, including both $^{1}$H and $^{31}$P metabolites. The scores plot clearly shows a tendency for separate clustering by the three treatment groups: normothermia (blue), hypothermia that starts with OGD (black), and hypothermia that starts after a 15-minute delay (red). The *x* and *y* axes of the plot are the two 'principal component' axes. Figure 4B shows the *loadings plot* (Eriksson *et al*, 2006) that corresponds to the *scores plot*. Metabolites in each quadrant of the loadings plot correspond to points in the same quadrant of the scores plot. Metabolites that are close together on the loadings plot are highly correlated, and metabolites furthest from the origin contributed most to the furthest points in the scores plot. For example, lactate and alanine are close to each other in the lower left quadrant of the plot, as are glycerophosphocholine and glycerophosphoethanolamine, and ATP and ADP in other quadrants, and each of these metabolites was influential in the scores plot.

### Terminal Deoxynucleotidyl Transferase-Mediated 2'-Deoxyuridine 5'-Triphosphate-Biotin Nick End Labeling Staining and Enzyme-Linked Immunosorbent Assay DNA Fragmentation Assay

The TUNEL-positive cells, which contain DNA fragmentation, were too few for cell counting. Figure 5 illustrates the help provided by costaining with propidium iodide in discerning when morphology in TUNEL-positive cells was suggestive of apoptosis (condensed, fragmented nuclei) and necrosis (diffusely stained nuclei). The ELISA DNA fragmentation quantifications, also in Figure 5, show that both at the end of the experiment and also at the time when hypothermia had been completed, cell death was significantly lower in the hypothermia group compared with the normothermia and delayed hypothermia groups, which had statistically similar values. In contrast, at the end of OGD, the normothermia group had significantly greater death than either of the two lower temperature groups, which had statistically similar values.

### Metabolomic Analyses II: L1-Penalized Regression

Cross-validation prediction error (CVPE) profiles from applying L1-penalized regression to $\beta$ATP and apoptotic cell death are given in Figures 6A and 6B, respectively. (This analysis did not include $^{31}$P-based metabolites.) As noted earlier, in this analysis, data are pooled from each of the four repetitions of three groups, each with three time points. Thus, the sample size had 36 data sets, which is close to the number of NMR-determined metabolites. The

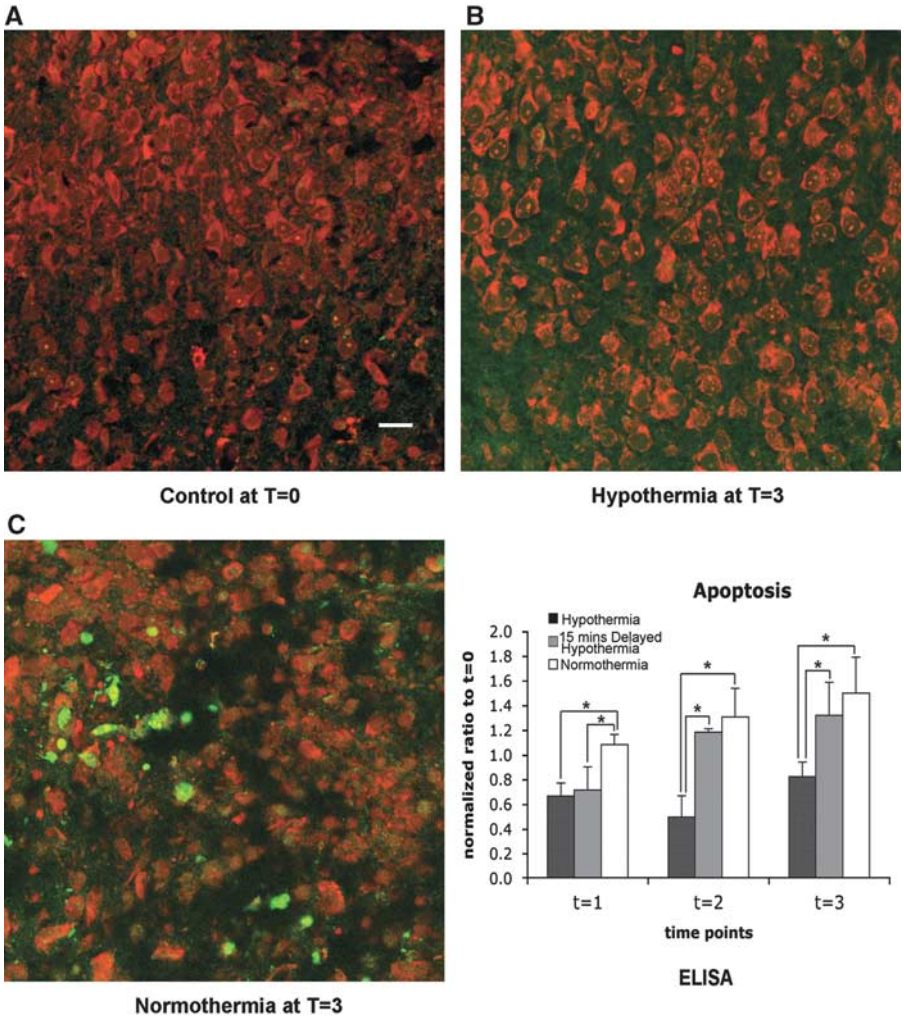


**Figure 5** Representative slice sections obtained with fluorescence confocal microscopy and double stained with propidium iodide (red) and the terminal deoynucleotidyl transferase-mediated 2'-deoxyuridine 5'-triphosphate-biotin nick end labeling (TUNEL) stain (green). Compared with control (**A**), cells in the hypothermia group (**B**) were only slightly more swollen, and generally of the same appearance. In contrast, cells of the normothermia group (**C**) showed greater deterioration. The TUNEL-positive cells were too few to count and were primarily in the normothermia group. Instead of cell counting, an enzyme-linked immunosorbent assay (ELISA) sensitive to DNA fragmentation was used, as described in the text. The bar graph at the lower right shows ELISA quantifications ($N = 3$), with cell death clearly greater at the end of the experiment for both the normothermia and delayed hypothermia groups, these having equal death within experimental errors. Statistical analysis included an analysis of variance to rule out null hypothesis, followed by the Fisher's protected least significant difference *post hoc* test. Data represent mean ± s.d. Asterisks indicate $P < 0.05$ significance.

number of variables chosen for calculating CVPE is plotted along the *x* axis as 'the fraction,' which is the ratio of the number of chosen variables to the total number of available variables (39 $^1$H metabolites). The *y* axis gives the CVPE obtained when the number of independent variables is that indicated by the corresponding value on the *x* axis. Thus, the ELISA outcome results are best fit when the NMR data set is taken to have six variables ($x = 0.15$, with 39 variables), whereas the $\beta$ATP outcome results suggest that as many as 12 variables are needed for a best fit. Both profiles are prototypic in that they exhibit initial decreases in CVPE as the value of 'fraction' starts to increase from 0 as important metabolites are entered; and then show almost no CVPE changes with further increases in 'fraction,' indicating that several statistical models attain approximately equal and minimal CVPE; and finally show ever increasing values of CVPE as noise variables are included. Several heuristics have been advanced for selecting a specific model based on such profiles. These include taking the number of metabolites to be that associated with minimum CVPE, or by finding a smaller model (fewer metabolites) by taking the smallest number of metabolites associated with a CVPE value that is within one standard error of the minimum CVPE. With $\beta$ATP as the outcome variable, the top five metabolites were PCr (as seen in $^1$H spectra), ATP-$^1$H, choline, formate, and phosphoethanolamine. The next five metabolites

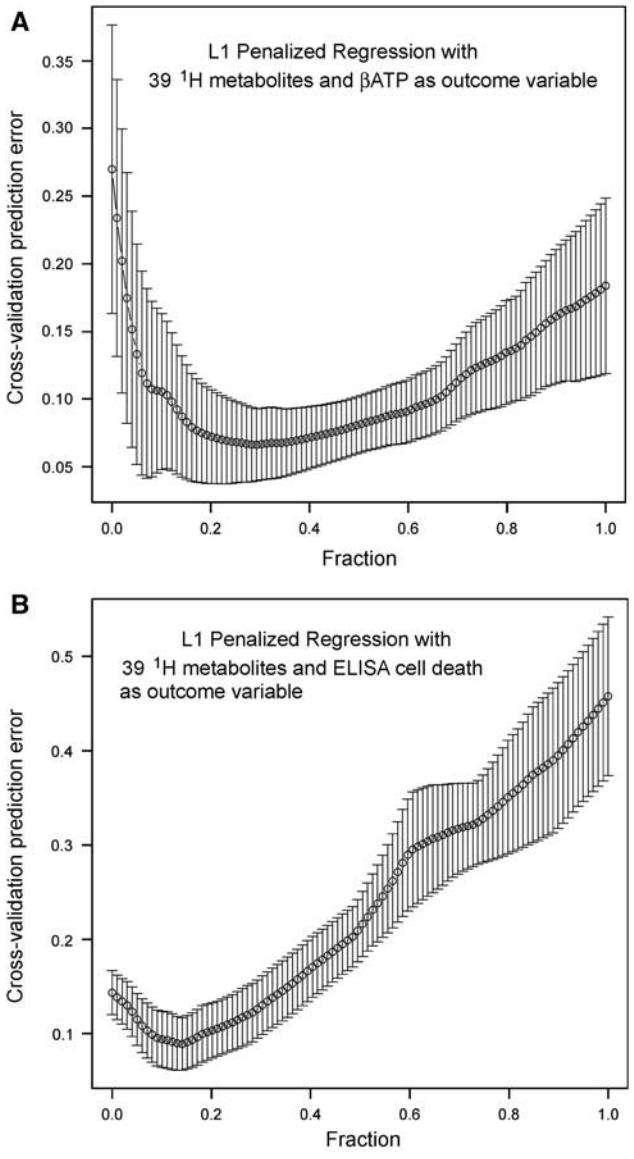


**Figure 6** Cross-validation prediction error (CVPE) profiles. Separate analysis was performed for each of the two outcome variables, these being the ratio of final to initial ATP (**A**), and the enzyme-linked immunosorbent assay (ELISA) cell-death quantification (**B**). In each analysis, all data from all time points were processed in an L1-penalized regression. The *y* axis gives the CVPE that results when the model tries having *n* independent metabolite variables to fit the data, with *n* being the abscissa along the *x* axis. Instead of being given as an integer, *n* is given as a fraction of the total number of metabolites. Thus in (**B**), the lowest CVPE value corresponds to the 'fraction' being 0.154, which in turn corresponds to having the outcome variable dominated by the behavior of six metabolites, when data for 39 metabolites are the input to the analysis. For each value of CVPE, one can look up which metabolites were found to be most important.

that would be allowed by going lower in 'fraction' are malate, fumarate, ADP-$^{1}$H, threonine, and glutathione. With the ELISA measure of cell death as the outcome variable, the top five metabolites were: ADP-$^{1}$H, valine, acetate, tryptophan, and formate, with these followed by phosphocreatine and leucine. In the analysis where cell death was the outcome variable, the inclusion of $^{31}$P-based metabolites did not change the results.

### *In Situ* Superoxide Production

Figure 7A shows selective, high-magnification confocal fluorescence imaging of superoxide, detected from its oxidation of HEt to Et (red fluorescence). Cross-sections 0.1 $\mu$m thick are shown through central slice regions, with cell nuclei appearing blue from 4′,6′-diamidino-2-phenylindole staining. Figure 7B plots superoxide quantifications for the hypothermia and normothermia groups, obtained for four time points as described in the Materials and methods. Superoxide, which barely existed in control slices, became incrementally greater with time, and always more so in the normothermia group.

## Discussion

Our brain slice preparation's advantages for modeling neonatal asphyxia include: that its neuron-glia architecture is close to that found *in vivo*, that the arrangement very conveniently accommodates ultra rapid freeze clamping of metabolites and cellular processes, and that it is easy to have tight control of $PO_2$, $PCO_2$, pH, temperature, and superfusate composition. We chose a hypoxia protocol with continuous superfusate flow, as continuous brain tissue perfusion is a key feature of the widely used Vannucci–Rice *in vivo* model of neonatal asphyxia (Vannucci *et al*, 1999; Vannucci and Vannucci, 2005). Glucose is well known to provide enormous anoxic protection to rat astrocytes during early development. In one astrocyte, cell culture study using 15 mmol/L glucose, 24 hours of total oxygen deprivation produced zero cell death (Callahan *et al*, 1990). Because of this and preclinical rodent studies that found decreases in both brain and plasma glucose during asphyxia (Basu *et al*, 2009; Holowach-Thurston *et al*, 1974), we felt that glucose deprivation was appropriate in our model. A disadvantage of acute brain slice preparations is that treatment times and post-insult recovery times are short compared with those for *in vivo* studies, where multiple mechanisms contribute to cell death. If, however, early, distinct metabolomic differences are seen clearly, it will be reasonable to look for such differences *in vivo*.

Knowing that almost all chemical reactions are affected by temperature changes, we felt that a multivariate metabolomic approach with simultaneous monitoring of 30 to 40 metabolite concentrations would lead to group parameters that distinguished metabolite ensembles associated with less injury and better outcomes. Despite our having far fewer data points per treatment group than used in traditional multivariate studies, the scores plots of

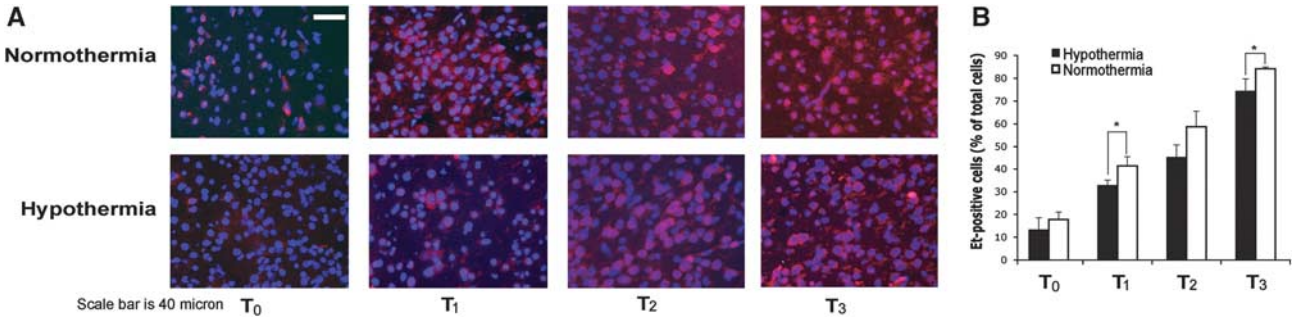


**Figure 7** (**A**) Comparison of ethidium (Et) fluorescence (red) with 4′,6′-diamidino-2-phenylindole (blue) nuclear counterstaining. (**B**) The graph at the right compares quantifications ($N = 4$ for each $T$) of red relative to blue for the four-slice sampling time points. Data represent mean ± s.d. ($n = 4$). Asterisks indicate significance compared with the normothermia group by the unpaired $t$-test. $P < 0.05$.

the PLS-DA showed clear separations, suggesting that multivariate characterizations are potentially useful. This phenomenon has been demonstrated previously in earlier works by us and others (Liu *et al*, 2009; Serkova and Niemann, 2006*a*; Serkova *et al*, 2006*b*; Jordan *et al*, 2009). Naturally, one expects that future accumulations of many more data points would lead to overlapping distributions, despite the cluster shrinkage and higher resolution of cluster separations provided by going from the PCA to a PLS-DA analysis. The separation of treatment groups on a metabolomics PLS-DA plot, however, is not the final step.

Although particular treatment groups might form distinguishable clusters on scores plots that possibly end up being consistently associated with better or worse biological outcomes, an analysis is needed that starts with outcome values and assesses the extent to which they were optimized by all or some of the biomarkers. The L1-penalized regression analysis, which for reasons already given was used instead of a PLS-DA or partial least squares regression (Eriksson *et al*, 2004; Wold *et al*, 2001), produced impressive differences with the two outcome variables that we chose: early cell death as measured by an ELISA, and ATP preservation, as measured by $^{31}$P NMR spectroscopy (while excluding all other $^{31}$P NMR data). Although the use of the ELISA assay as an outcome variable worked well in this particular study, interpretations of ELISA quantifications in this study is limited by a lack of calibration. The ELISA changes are measured relative to baseline values, not relative to the maximal apoptotic stimulus. Thus, if overall cell death is small at baseline, for example 10%, a 40% increase in ELISA represents only a 4% increase in overall cell death.

It is easy to conclude that taking ATP preservation as the sole outcome variable would not be very helpful in our model, as the two hypothermia treatment groups totally restored their initial high-energy phosphates while having large differences in early cell death. This is also apparent from the L1-penalized regression, which found that 12 metabolites of 39 $^{1}$H metabolites were very important to ATP optimization. In contrast, early cell death had significant differences between the two hypothermia treatment groups with only six key metabolites, with two being $^{1}$H-detected high-energy phosphates. The data support the notion that early ATP recovery does not imply that all is well at cellular levels. Although ATP preservation after 6 hours of recovery, the time when our experiments finished, might not be very helpful as an outcome variable, in experiments that go out to much later times it might nevertheless have associations more meaningful than those of ELISA measurements, which are based on caspase-initiated endonuclease cleavage at internucleosomal linker regions (presumably before ATP depletion). After 6 hours of recovery, ELISA measurements might account for only a fraction of the dying neurons. After OGD, eventual ATP depletion from necrosis and caspase-independent pathways can be more prominent at later times, as noted in two earlier studies (Bonfoco *et al*, 1995; Kalda *et al*, 1998).

From a metabolomic perspective, the data suggest that the detection of 'downfield' $^{1}$H metabolites ($^{1}$H resonances to the left of the $H_2O$ peak) can add much to metabolic monitoring and predicting. Such, of course, is very easy in extract spectra, and much more challenging *in vivo*. Nevertheless, data have appeared that show *in vivo* detection with current techniques is within reach (Vermathen *et al*, 1999), and that accurate *ex vivo* detection in tissues is more easily attainable (Fris and Midelfart, 2007). As acquisition of $^{31}$P NMR spectra can easily require times that are longer by a factor $\geqslant 10$, it would be very significant to be able to obtain the same or better analyses with only $^{1}$H data.

We considered treating superoxide quantifications as an outcome variable or an additional biomarker measure of insult, but had to hold back because HEt fluorescence detection of superoxide is so sensitive a technique, that noninjurious perturbations, such as isoflurane anesthesia with no insult, can produce HEt images similar to those in this paper (Tanaka *et al*, 2003). We also considered having an experimental group in which therapeutic hypothermia was initiated at the end of the 45-minute OGD period. Preliminary data (not shown) strongly suggested, as might be surmized from Figure 3, that one would not

find this group's ATP results to be distinguishable from the normothermia results.

In conclusion, in the presented OGD brain slice model of neonatal asphyxia, normothermic tissue suffered ATP losses and cell death, but tissue given a 4°C temperature decrease preserved ATP levels, whether the temperature change was applied at the start of OGD or 15 minutes later. However, cell death was substantially reduced only when the temperature decrease was simultaneous with the OGD onset. Although the metabolomic analyses found that the different treatment groups were forming separate clusters, larger data samples and improved choices of outcome variables are needed for further mechanistic insight.

## Disclosure/conflict of interest

The authors declare no conflict of interest.

## Appendix on the Arrhenius equation

Many preclinical studies have found that after brain hypoxia/ischemia, outcomes can be dramatically improved by mild therapeutic hypothermia, with temperature decreases typically of only 4°C. Given that body chemistry is occurring at an absolute temperature of ~309°K, a 4°C decrease is only a 1.3% change. What makes it possible for small temperature changes to be so important?

The answer can be found in the Arrhenius equation for the rate constant $K$ of any chemical reaction A→B:
$K = (\text{a constant}) \times \exp([-\text{activation energy}]/[kT])$

The 'activation energy' normally equals the threshold energy, because contributions from the mean thermal energy are normally extremely small compared with reaction energies (Menzinger and Wolfgang, 1969). In such situations, the activation energy does not change with temperature, and the rate constant has exponential behavior with $(1/T)$. Earlier studies based on temperature independence of the activation energy found that a decrease of 4°C would lower the human cerebral metabolic rate by ~28% (taking $Q10 = 2.3$), and the rat cerebral metabolic rate by 63% (taking $Q10 = 12$). However, near reaction thresholds the activation energy can be a function of temperature, and dramatic reaction rate changes can occur within a 4°C temperature interval, if chemical reaction thresholds are crossed in that interval. If, for example, the increase of a few degrees allows greater opening of hundreds of hydrogen bonds, reactions that depend on those bond openings will be greatly facilitated.

## References

Basu P, Som S, Choudhuri N, Das H (2009) Contribution of the blood glucose level in perinatal asphyxia. *Eur J Pediatr* 168:833–8

Berthet C, Lei H, Thevenet J, Gruetter R, Magistretti PJ, Hirt L (2009) Neuroprotective role of lactate after cerebral ischemia. *J Cereb Blood Flow Metab* 29:1780–9

Bonfoco E, Krainc D, Ankarcrona M, Nicotera P, Lipton SA (1995) Apoptosis and necrosis: two distinct events induced, respectively, by mild and intense insults with N-methyl-D-aspartate or nitric oxide/superoxide in cortical cell cultures. *Proc Natl Acad Sci USA* 92:7162–6

Callahan DJ, Engle MJ, Volpe JJ (1990) Hypoxic injury to developing glial cells: protective effect of high glucose. *Pediatr Res* 27:186–90

Compagnoni G, Bottura C, Cavallaro G, Cristofori G, Lista G, Mosca F (2008) Safety of deep hypothermia in treating neonatal asphyxia. *Neonatology* 93:230–5

Compagnoni G, Pogliani L, Lista G, Castoldi F, Fontana P, Mosca F (2002) Hypothermia reduces neurological damage in asphyxiated newborn infants. *Biol Neonate* 82:222–7

Dagia C, Ditchfield M (2008) 3T MRI in paediatrics: challenges and clinical applications. *Eur J Radiol* 68:309–19

De Vita E, Bainbridge A, Cheong JL, Hagmann C, Lombard R, Chong WK, Wyatt JS, Cady EB, Ordidge RJ, Robertson NJ (2006) Magnetic resonance imaging of neonatal encephalopathy at 4.7 Tesla: initial experiences. *Pediatrics* 118:e1812–21

Efron B, Hastie T, Johnstone I, Tibshirani R (2004) Least angle regression. *Ann Stat* 32:407–99

Eriksson L, Antti H, Gottfries J, Holmes E, Johansson E, Lindgren F, Long I, Lundstedt T, Trygg J, Wold S (2004) Using chemometrics for navigating in the large data sets of genomics, proteomics, and metabonomics (gpm). *Anal Bioanal Chem* 380:419–29

Eriksson L, Johansson E, Kettaneh-Woldn N, Trygg J, Wikstrom C, Wold S (2006) *Multi and Megavariate Data Analysis: Parts I and II*. 2nd ed. San Jose, CA: Umetrics

Espanol MT, Litt L, Yang GY, Chang LH, Chan PH, James TL, Weinstein PR (1992) Tolerance of low intracellular pH during hypercapnia by rat cortical brain slices: a $^{31}P/^{1}H$ NMR study. *J Neurochem* 59:1820–8

Fris M, Midelfart A (2007) Postnatal biochemical changes in rat lens: an important factor in cataract models. *Curr Eye Res* 32:95–103

Gluckman PD, Wyatt JS, Azzopardi D, Ballard R, Edwards AD, Ferriero DM, Polin RA, Robertson CM, Thoresen M, Whitelaw A, Gunn AJ (2005) Selective head cooling with mild systemic hypothermia after neonatal encephalopathy: multicentre randomised trial. *Lancet* 365:663–70

Goeman JJ (2010) L1 penalized estimation in the Cox proportional hazards model. *Biom J* 52:70–84

Govindaraju V, Young K, Maudsley AA (2000) Proton NMR chemical shifts and coupling constants for brain metabolites. *NMR Biomed* 13:129–53

Gunn AJ, Gluckman PD, Gunn TR (1998) Selective head cooling in newborn infants after perinatal asphyxia: a safety study. *Pediatrics* 102:885–92

Hastie T, Tibshirani R, Friedman J (2010) *The Elements of Statistical Learning: Data Mining, Inference, and Prediction*. 2nd ed. New York: Springer

Holowach-Thurston J, Hauhart RE, Jones EM (1974) Anoxia in mice: reduced glucose in brain with normal or elevated glucose in plasma and increased survival after glucose treatment. *Pediatr Res* 8:238–43

Jordan KW, Nordenstam J, Lauwers GY, Rothenberger DA, Alavi K, Garwood M, Cheng LL (2009) Metabolomic characterization of human rectal adenocarcinoma with intact tissue magnetic resonance spectroscopy. *Dis Colon Rectum* 52:520–5

Kalda A, Eriste E, Vassiljev V, Zharkovsky A (1998) Medium transitory oxygen-glucose deprivation induced both apoptosis and necrosis in cerebellar granule cells. *Neurosci Lett* 240:21–4

Lei H, Poitry-Yamate C, Preitner F, Thorens B, Gruetter R (2010) Neurochemical profile of the mouse hypothalamus using *in vivo* $^{1}$H MRS at 14.1T. *NMR Biomed* 23:578–83

Leist M, Kühnle S, Single B, Nicotera P (1998) Differentiation between apoptotic and necrotic cell death by means of the BM cell death detection ELISA or annexin V staining. *Biochemica* 2:25–8

Liu J, Hirai K, Litt L (2008) Fructose-1,6-bisphosphate does not preserve ATP in hypoxic-ischemic neonatal cerebrocortical slices. *Brain Res* 1238:230–8

Liu J, Segal M, Yoo S, Yang GY, Kelly M, James TL, Litt L (2009) Antioxidant effect of ethyl pyruvate in respiring neonatal cerebrocortical slices after $H_2O_2$ stress. *Neurochem Int* 54:106–10

Menzinger M, Wolfgang R (1969) The meaning and use of the Arrhenius activation energy. *Angew Chem* 8:438–44

Mlynarik V, Cudalbu C, Xin L, Gruetter R (2008) $^{1}$H NMR spectroscopy of rat brain *in vivo* at 14.1Tesla: improvements in quantification of the neurochemical profile. *J Magn Reson* 194:163–8

Pettegrew JW, Keshavan MS, Minshew NJ (1993) $^{31}$P nuclear magnetic resonance spectroscopy: neurodevelopment and schizophrenia. *Schizophr Bull* 19:35–53

Serkova NJ, Niemann CU (2006*a*) Pattern recognition and biomarker validation using quantitative 1H-NMR-based metabolomics. *Expert Rev Mol Diagn* 6:717–31

Serkova NJ, Jackman M, Brown JL, Liu T, Hirose R, Roberts JP, Maher JJ, Niemann CU (2006*b*) Metabolic profiling of livers and blood from obese Zucker rats. *J Hepatol* 44:956–62

Shankaran S, Laptook AR, Ehrenkranz RA, Tyson JE, McDonald SA, Donovan EF, Fanaroff AA, Poole WK, Wright LL, Higgins RD, Finer NN, Carlo WA, Duara S, Oh W, Cotten CM, Stevenson DK, Stoll BJ, Lemons JA, Guillet R, Jobe AH (2005) Whole-body hypothermia for neonates with hypoxic-ischemic encephalopathy. *N Engl J Med* 353:1574–84

Tanaka K, Weihrauch D, Ludwig LM, Kersten JR, Pagel PS, Warltier DC (2003) Mitochondrial adenosine triphosphate-regulated potassium channel opening acts as a trigger for isoflurane-induced preconditioning by generating reactive oxygen species. *Anesthesiology* 98:935–43

Tibshirani R (1996) Regression shrinkage and selection via the LASSO. *J Roy Stat Soc B (Stat Methodol)* 58:267–88

Vannucci RC, Connor JR, Mauger DT, Palmer C, Smith MB, Towfighi J, Vannucci SJ (1999) Rat model of perinatal hypoxic-ischemic brain damage. *J Neurosci Res* 55:158–63

Vannucci RC, Vannucci SJ (2005) Perinatal hypoxic-ischemic brain damage: evolution of an animal model. *Dev Neurosci* 27:81–6

Vermathen P, Govindaraju V, Matson GB, Maudsley AA (1999) Detection of downfield $^{1}$H resonances in human brain using single voxel and SI methods. *Seventh Meeting Proc ISMRM*, pp 1584

Weljie AM, Newton J, Mercier P, Carlson E, Slupsky CM (2006) Targeted profiling: quantitative analysis of $^{1}$H NMR metabolomics data. *Anal Chem* 78:4430–42

Willker W, Engelmann J, Brand A, Leibfritz D (1996) Metabolite identification in cell extracts and culture media by proton-detected 2D [$^{1}$H, $^{13}$C] NMR spectroscopy. *J Magn Res Anal* 2:21–32

Wold S, Sjöström M, Eriksson L (2001) PLS-regression: a basic tool of chemometrics. *Chem Intell Lab Syst* 58:109–30

Zeng J, Liu J, Yang GY, Kelly MJ, James TL, Litt L (2007) Exogenous ethyl pyruvate versus pyruvate during metabolic recovery after oxidative stress in neonatal rat cerebrocortical slices. *Anesthesiology* 107:630–40